Volume Dependence of Hydrogen Sorption and Desorption Diffusion in Cylindrical Polymers

Jae Kap Jung (jkjung@kriss.re.kr)
Korea Research Institute of Standards and Science
Kyu-Tae Kim
Korea Research Institute of Standards and Science
Un Bong Baek
Korea Research Institute of Standards and Science
Seung Hoon Nahm
Korea Research Institute of Standards and Science

Research Article

Keywords: Volume dependence, hydrogen sorption, desorption diffusion, cylindrical polymers, hydrogen molecules, numerical simulations

Posted Date: October 13th, 2021

DOI: https://doi.org/10.21203/rs.3.rs-957225/v1

Volume dependence of hydrogen sorption and desorption diffusion in cylindrical polymers

Jae Kap Jung[a,*], Kyu-Tae Kim[b], Un Bong Baek[a], and Seung Hoon Nahm[a]

[a]Hydrogen Energy Materials Research Center, Korea Research Institute of Standards and Science, Daejeon 34113, Korea

[b]Electricity and Magnetism Group, Korea Research Institute of Standards and Science, Daejeon 34113, Korea

***Corresponding author**

Hydrogen Energy Materials Research Center, Korea Research Institute of Standards and Science, Daejeon 34113, Korea

E-mail: jkjung@kriss.re.kr (Jae Kap Jung)

Tel: 82-42-868-5759

Fax: 82-42-868-5018

Abstract

We have investigated the volume effects on hydrogen diffusion properties in both sorption and desorption processes by employing a volumetric analysis technique. The total uptake (C_∞), total desorbed content (C_0), sorption diffusion coefficient (D_s), desorption diffusion coefficient (D_d), sorption and desorption equilibrium time of hydrogen in two rubbery polymers are determined relative to the diameter and thickness of the cylindrical sample in the two processes. C_∞ and C_0 do not demonstrate the appreciable volume dependence for all rubbers. The identical values in C_∞ and C_0 indicate the reversibility between sorption and desorption, which is interpreted by the occurrence of physisorption rather than chemisorption by introducing hydrogen molecules. The larger D_d values in the desorption process than D_s may be attributed to increased amorphous phase and volume swelling caused by increased hydrogen voids and polymer chain scission after decompression. The time to reach equilibrium in both sorption and desorption processes was found to be linearly proportional to the square of thickness above an aspect ratio of 3.7, which is consistent with the numerical simulations based on the solution of Fick's law. This finding could be used to predict the equilibrium adsorption time depending on the sample size in the polymer.

1. Introduction

Sorption is an important chemical process in solid membranes, and desorption is the reverse process and follows similar diffusion laws. Gas sorption and desorption are critical factors introduced to control the permeation property in sealing applications[1-3]. The permeation efficiency is related to not only the equilibrium features but also the kinetics of both processes under high-pressure environments[4,5]. In particular, an investigation of the saturated equilibrium and related physical stability in hydrogen permeation is essential for designing industrial equipment, reducing operating costs, gaining insights into adsorption and finally determining the appropriate exposure time to hydrogen under high pressure in cycling testing[6,7].

The permeability properties are evaluated by various methods, such as gravimetric techniques[8], the magnetic suspension balance method[9], manometric methods[10], constant pressure methods[11] and thermal desorption analysis[12]. Gas diffusion properties and equilibrium time have certainly been affected by the sample shape and volume. However, most evaluation techniques have limitations in determining the permeation parameters according to variations in the shape and size of the sample employed. Furthermore, researches have mainly focused on the hydrogen effects of the physical, thermal and mechanical properties after pressurization and then decompression[13-15]; however, *in situ* measurements during pressurization under high pressures have rarely been conducted.

To supplement and extend the previous limited research, we investigated the hydrogen sorption property in the process of pressurization, together with the volume dependence of the permeation parameters for cylindrical samples with different diameters and thicknesses. The developed volumetric analysis technique (VAT)[16,17] is appropriate in these experimental investigations. This research was conducted for rubbery polymers, such as nitrile butadiene

rubber (NBR) and ethylene propylene diene monomer (EPDM), which are utilized as sealing materials for O-rings in gas applications, such as hydrogen fueling stations[18].

The main concern of present research is based on the general behavior in the sorption and desorption properties of hydrogen in polymers in terms of hydrogen uptake and diffusion coefficient from investigation results of volume dependence obtained for the same materials. The sorption and desorption equilibrium time is important for determining the high-pressure exposure conditions in the cycling test of rubbers and designing the O-ring material for the high-pressure hydrogen gas sealing devices. The time to reach sorption and desorption equilibrium is found to be directly dependent on both the sample volume, diffusion coefficient and aspect ratio of the cylindrical sample. The equilibrium time evaluated by experimental investigations is confirmed by performing numerical simulations based on the solution of Fick's law. Thus, the sorption equilibrium time required to design O-ring seals can be predicted.

2. Volumetric analysis technique and measuring principle

The chemical composition of the rubber investigated in this research is found in liteatures[16,17]. The experiments were conducted after exposure and subsequent decompression. The polymer specimen was exposed to a fixed pressure of 5.75 MPa for the required residence time. After decompression to atmospheric pressure, hydrogen gas from the rubber was released. Subsequently, the polymer from the high-pressure chamber was loaded into the graduated cylinder of the VAT system, as shown in Fig. 1.

The simple VAT system shown in Fig. 1(a) measured the released hydrogen. A graduated cylinder immersed partially in a water container collected and measured the emitted H_2 gas with an O-ring to prevent gas leakage. Figure 1(b) shows a photograph of a stretched graduated cylinder

with a volume capacity of 20 ml, with the volume depending on the desorbed hydrogen gas content versus pressure. The graduated cylinder fabricated by transparent acrylic was employed to clearly observe the water level. The water level was precisely measured with a resolution of 0.01 ml by a digital camera or two electrodes in real time at specified time intervals for the case with a volume capacity of 10 ml.

The pressure (P) inside the graduated cylinder for hydrogen gas measurement, as shown in Fig. 1(a), is expressed as follows[17]:

$$P = P_o - \rho g h \quad (1)$$

where P_o is the outside atmosphere pressure of the cylinder, ρ is the density of distilled water in the water container, g is gravity and h is the height of the distilled water level indicated by the blue part in Fig. 1(a) inside the graduated cylinder measured from the water level in the water container. As shown in Fig. 1(a), the hydrogen gas released from the rubber after decompression lowers the water level of the cylinder, which is governed by the ideal gas equation, $PV=nRT$, where R is the gas constant with 8.20544×10^{-5} m^3·atm/(mol·K), V is the volume inside the graduated cylinder filled with gas, and n is the number of hydrogen gas moles. Thus, we could quantify the content of released hydrogen by measuring the change in the water level (ΔV).

The increased number of moles (Δn) of hydrogen gas collected inside the graduated cylinder was obtained by measuring the lowered water level ($\Delta V = A\Delta h$), i.e., volume change (ΔV) due to hydrogen emitted from rubber at specified P and T as follows[17]:

$$\Delta n = \frac{(P_o - \rho g h) A \Delta h}{RT} \quad (2)$$

where A is the cross-sectional area of the cylinder and Δh is the water level lowered by released hydrogen. The increased number of moles (Δn) of hydrogen gas is converted to mass concentration $[C(t)]$ in the rubber sample as follows:

$$C(t)[\mathrm{wt}\cdot\mathrm{ppm}] = \Delta n[\mathrm{mol}] \times \frac{2.016\,[\frac{\mathrm{g}}{\mathrm{mol}}]}{m_{sample}[\mathrm{g}]} \quad (3)$$

where 2.016 [g/mol] is the molar mass of hydrogen and m_{sample} is the mass of the polymer. Therefore, the time-dependent mass concentration is obtained by measuring the water level change, Δh, versus the elapsed time after decompression.

Assuming that the adsorption and desorption of H_2 is a diffusion-controlled process, the emitted H_2 content $C_E(t)$ in the adsorption process and remaining H_2 mass concentration $C_R(t)$ in the desorption process are expressed as (4) and (5), respectively[19,20]:

$$C_E(t)/C_\infty = 1 - \frac{32}{\pi^2} \times \left[\sum_{n=0}^{\infty} \frac{exp\left\{\frac{-(2n+1)^2\pi^2 D_s t}{l^2}\right\}}{(2n+1)^2}\right] \times \left[\sum_{n=1}^{\infty} \frac{exp\left\{-\frac{D_s\beta_n^2 t}{\rho^2}\right\}}{\beta_n^2}\right] \quad (4)$$

$$C_R(t) = \frac{32}{\pi^2} \times C_0 \times \left[\sum_{n=0}^{\infty} \frac{exp\left\{\frac{-(2n+1)^2\pi^2 D_d t}{l^2}\right\}}{(2n+1)^2}\right] \times \left[\sum_{n=1}^{\infty} \frac{exp\left\{-\frac{D_d\beta_n^2 t}{\rho^2}\right\}}{\beta_n^2}\right] \quad (5)$$

Equations (4) and (5) are the solutions to Fick's second diffusion law for a cylindrical sample. A constantly uniform hydrogen concentration is initially maintained, and the cylindrical surfaces are kept at a constant concentration. In equations (4) and (5), l is the thickness of the cylindrical rubber sample, ρ is the radius, and β_n is the root of the zero-order Bessel function.

In equation (4), C_∞ is the saturated hydrogen mass at an infinitely long time, i.e., the total emitted mass concentration or hydrogen uptake in the sorption process, and in equation (5), C_0 is the remaining mass concentration at t =0 in the desorption process, that is, the total desorption content. In addition, D_s and D_d are the diffusion coefficients of sorption and desorption, respectively.

To analyze the time-varying mass concentration data with a form of a multiexponential function, we used a diffusion analysis program developed using Visual Studio to calculate D_s,

D_d, C_∞ and C_0 in equations (4) and (5) based on the least-squares regression method[17,21].

3. Sequence for measuring sorption and desorption diffusion

The elapsed time after decompression is counted from the moment (t=0) at which the high-pressure chamber is reduced to atmospheric pressure. The released content obtained from the measurement is regarded as the sorption content of hydrogen because all entering hydrogen was entirely emitted.

The sequence for measuring the sorption and desorption diffusion parameters is displayed in Fig. 2(a) and (b), respectively. The hydrogen sorption contents are measured as a function of residence time (exposed time) of specimens exposed to a high-pressure chamber using VAT. The sorption quantity in unit of hydrogen mass concentration in equation (3) versus elapsed time obtained by VAT after decompression exposed at a single residence time, a, is shown in step a of Fig. 2(a). As a result of this measurement, $c_0(t = \mathrm{a})$ at time a is obtained by equation (5). As shown in step b of Fig. 2(a), $c_0(t = \mathrm{b})$ at time b is obtained by equation (5) after decompression for exposure at residence time b. The c_0 varying residence times (time a, b, …, j) are collected until hydrogen sorption equilibrium arrives. Thus, the sorption data array is obtained from a series of measurements of desorption after subsequent exposure times. From the c_0 versus the exposed time shown in Fig. 2(a), the C_∞ and D_s of hydrogen are determined by applying the diffusion analysis program based on equation (4) to the measured results. The sequence for measuring the sorption properties takes a quite long time to complete.

In the case of the desorption process in Fig. 2(b), the hydrogen desorption content and diffusivity are determined from a single measurement after decompression for exposure to a sufficiently long equilibrium sorption time for the specimens under a high-pressure chamber.

From the desorption data shown in Fig. 2(b), we can determine C_0 and D_d by fitting with equation (5). Thus, desorption is an easier process to complete because the measurement requires one step with one sample.

4. Results and discussion

The hydrogen diffusion properties in the two processes are measured according to the sorption and desorption procedure in Figs. 2. Fig. 3 shows the investigation results of hydrogen sorption (C_∞) and desorption content (C_0) for cylindrically shaped NBR and EPDM with different diameters and thicknesses. The values of C_∞ and C_0 are analyzed by equations (4) and (5), respectively, using the diffusion analysis program.

The general behavior illustrated in Fig. 3(a) and (b) for the NBR and EPDM, respectively, is as follows: both the total sorption content, C_∞, and the total desorption content, C_0, in each rubber are consistent regardless of the sample diameter and thickness. As shown in Fig. 3(a), the average C_∞ and C_0 values (284 wt·ppm) in the NBR are equivalent within the uncertainty range. As shown in Fig. 3(b), the average C_∞ and C_0 values (242 wt·ppm) in the EPDM are also equivalent within the uncertainty range. This finding indicates that the sorption and desorption processes of hydrogen in the NBR and EPDM are reversible because physisorption rather than chemisorption occurs by introducing hydrogen. This result is consistent with previous reports showing that high-pressure hydrogen exposure does not cause any chemical structure changes in NBR by nuclear magnetic resonance analysis[22,23]. The reversible adsorption phenomenon of hydrogen is usually observed in the literature[24,25]. In particular, in hydrogen storage materials, reversibility is defined as its ability to retain its storage capacity during repeated hydrogen charge and discharge in long-term cycling stability, and it represents an important quantity.

Meanwhile, the hydrogen diffusivity versus diameter and thickness of the sample for two processes are shown in Fig. 4. The values of D_s and D_d are also analyzed by equations (4) and (5), respectively, with the diffusion analysis program. The sorption and desorption diffusivity displays a slight volume dependence above a thickness of 5 mm. The thickness of the sample during diffusion is a more sensitive factor than the diameter. The investigation results in Fig. 4 indicate that the desorption diffusion coefficient D_d is higher than D_s in the sorption process for both rubbers. The hysteresis in diffusion observed between the two processes means that the sorption and desorption mechanisms are different from each other. The sorption and desorption hysteresis may be significantly attributed to the increase in hydrogen diffusion due to rapid decompression yielding expanded hydrogen voids and volume swelling. Furthermore, hydrogen penetration causes scission of the polymer chain and diffusion takes place in the amorphous region, as indicated in the literature[26,27].

Furthermore, the sorption and desorption curves have a multiexponential form with varying time. Thus, the equilibrium time in the two processes is defined as the time at which the hydrogen content reaches 97% of the total sorption content, i.e., $C(t)$=0.97 for C_∞ and 3% for the total desorption content, i.e., $C(t)$=0.03 for C_0. Figure 5(a) and (b) display the curves of normalized sorption content versus exposed time and normalized desorption content versus time after decompression, respectively, with varying diameters at a fixed thickness of 2.5 mm for NBR. As shown in Fig. 5(a), the corresponding sorption equilibrium times (blue arrow) obtained for NBR are 26,338 s for a diameter of 5 mm and thickness of 2.5 mm, 37,338 s for a diameter of 10 mm and thickness of 2.5 mm, and 36,562 s for a diameter of 14 mm and thickness of 2.5 mm. Meanwhile, the desorption equilibrium times (blue arrow) determined for NBR in Fig. 5(b) are 21,738 s for a diameter of 5 mm and thickness of 2.5 mm, 32,792 s for a diameter of 10 mm and

thickness of 2.5 mm, and 30,987 s for a diameter of 14 mm and thickness of 2.5 mm.

Figure 6(a) and (b) show the normalized sorption and desorption curves versus time, respectively, with varying thicknesses and similar diameters for NBR. The corresponding sorption equilibrium times (blue arrow) obtained for NBR are 36,562 s for a diameter of 14 mm and thickness of 2.5 mm, 124,905 s for a diameter of 12 mm and thickness of 5 mm, and 178,986 s for a diameter of 12 mm and thickness of 10 mm. The desorption equilibrium times (blue arrow) obtained for NBR are 30,987 s for a diameter of 14 mm and thickness of 2.5 mm, 60,777 s for a diameter of 12 mm and thickness of 5 mm, and 124,193 s for a diameter of 12 mm and thickness of 10 mm. EPDM also displays a similar volume dependence for equilibrium time as NBR. The equilibrium time in EPDM is faster compared to that measured in NBR because of its faster diffusivity than NBR, as shown in Fig. 4.

We visualized the equilibrium time of sorption and desorption measured for cylindrically shaped NBR in Fig. 7(a) and (b), respectively, through a three-dimensional plot of the corresponding sorption and desorption equilibrium time versus diameter and thickness for NBR. The aspect ratio (AR=D/T) is defined as the diameter (D) with regard to the thickness (T) of the cylindrical sample. In the case of a thickness of 2.3 mm in Fig. 7(a) and (b), the sorption and desorption equilibrium time increases with increasing diameter up to an AR of 3.7 (slanted blue arrow) and is nearly constant above an AR of 3.7 (horizontal blue line). In the case of a thickness of 5.3 mm in Fig. 7(a) and (b), a similar diameter dependence as observed with a thickness of 2.3 mm is also found. In other words, the sorption and desorption equilibrium time increases with increasing diameter up to an AR of 3.7 and is nearly constant above an AR of 3.7. Meanwhile, the sorption and desorption equilibrium time increases with increasing thickness at a constant diameter. As expected in Fig. 4, the change in equilibrium time versus thickness is steeper than that observed

for diameter.

Similar to the NBR sample, we also visualized the equilibrium time of sorption and desorption for a cylindrically shaped EPDM with varying diameters or thicknesses. Fig. 8(a) and (b) show the three-dimensional plot of the corresponding sorption and desorption equilibrium time versus volume for EPDM. In the case of a thickness of 2.3 mm in Fig. 8(a) and (b), the sorption and desorption equilibrium time increases with increasing diameter up to an AR of 3.7 (slanted blue arrow) and is nearly constant above an AR of 4.0 (horizontal blue line). In the case of a thickness of 5.3 mm in Fig. 7(a) and (b), a similar diameter dependence is also found. Meanwhile, the sorption and desorption equilibrium time increases with increasing thickness at a fixed diameter. The change in equilibrium time versus thickness steepened compared with that observed for diameter.

After the investigations shown in Figs. 7 and 8, we focused on the sensitive thickness dependence on the equilibrium time of both the sorption and desorption processes for the two rubbers. Fig. 9(a) and (b) depict the saturation time for sorption/desorption equilibrium time versus square of the thickness for NBR and EPDM cylindrical shaped rubber, respectively. The experimental observation indicates that the thicker the sample is, the longer the time to reach hydrogen equilibrium saturation. The investigations clearly demonstrate a linear correlation between the saturation time and square of the thickness above an AR of 3.7 for both specimens. In Fig. 9(a), the black line indicates the linear relation between the sorption equilibrium time and square of thickness for NBR. In Fig. 9(a), the blue line indicates the linear relation between desorption equilibrium time and square of thickness for NBR. In Fig. 9(b), the black (blue) line indicates the linear relation between sorption (desorption) equilibrium time and square of thickness for EPDM. The reciprocal slope indicates the diffusion coefficient. The faster diffusion

coefficient for EPDM than NBR is attributed to the short equilibrium time, which corresponds to a small slope in the equilibrium time with regard to the square of the thickness.

In addition, the linearity deviates below an AR of 3.7 for both NBR and EPDM, as shown in ellipses with red oblique lines in Fig. 9.

To verify the linearity observed between the equilibrium time and square of thickness above an aspect ratio of 3.7, a numerical simulation based on the solution of Fick's law is conducted for the rubbers. Figure 10(a) presents the normalized hydrogen content for different thicknesses (T) with a diffusion coefficient (DC) of 5×10^{-11} m^2/s and diameter (D) of 20 mm. Panels a, b, c, d and e indicate the equilibrium times for thicknesses of 1 mm, 2 mm, 3 mm, 4 mm and 5 mm, respectively. Figure 10(b) is plotted from the simulation result of Fig. 10(a). The distinct linear dependence between the equilibrium time and square of thickness with a correlation coefficient R^2=0.998 is demonstrated, which is consistent with the experimental investigation, as shown in Fig. 9(a) and (b).

Moreover, Fig. 10(c) shows the numerical simulation of normalized hydrogen content for different diameters with a DC of 5×10^{-11} m^2/s and thickness (T) of 2.5 mm for the case above AR of 3.7. Panels a, b, c and d indicate the equilibrium time for diameters of 10 mm, 20 mm, 30 mm and 40 mm, respectively. The simulation result replotted in Fig. 10(d) indicates that the equilibrium time slightly increases with increasing radius.

5. Conclusions

By utilizing both the volumetric analysis technique and the established procedure for measuring the sorption parameters during pressurization, we characterize the sorption properties and desorption properties of hydrogen in two cylindrical rubbery polymers. The hydrogen content,

diffusion coefficient and equilibrium time versus sample volume are obtained for both the sorption and desorption processes. Volume dependence is not observed for C_0 and C_∞, whereas it is observed for D_s and D_d. The volume effect demonstrates that the thickness during diffusion is a more critical factor than the diameter of the specimen. The reversibility in hydrogen content observed between the sorption and sorption processes is ascribed to the occurrence of physisorption rather than chemisorption by the introduction of hydrogen.

The sorption and desorption equilibrium time is mainly affected by the following important factors: diffusion coefficient, sample thickness, and aspect ratio of the sample employed. An aspect ratio of approximately 3.7 is a critical region whether the equilibrium time is proportional to the square of the thickness above it or not below it. The aspect ratio of 3.7 is also a critical region whether the equilibrium time is nearly unaffected by a diameter above it or not below it.

The equilibrium time for polymers with different thicknesses at known diffusivities could be estimated from the linear relationship without experimental measurements, which was confirmed by predictive numerical simulations. Therefore, numerical simulations can be performed to predict the sorption equilibrium time for polymers and metals with any cylinder, sheet or sphere form.

Data availability

References

1. Lainé, E., Grandidier, J. C., Benoit, G., Omnès, B. & Boyer, S. A. E. Non-contact method used to determine the swelling/shrinking coefficients under CO_2 sorption/desorption on an HNBR O-ring - Study of coupling with temperature and pressure. *Polym. Test.* **85,** 106411 (2020).
2. Denis, N., Pone, J., Halleck, P. M. & Mathews, J. P. 3D characterization of coal strains induced by compression, carbon dioxide sorption, and desorption at in-situ stress conditions. *Int. J. Coal Geol.* **82,** 262-268 (2010).
3. Lainé, E., Grandidier, J. C., Benoit, G., Omnès, B. & Destaing, F. Effects of sorption and desorption of CO_2 on the thermomechanical experimental behavior of HNBR and FKM O-rings - Influence of nanofiller-reinforced rubber. *Polym. Test.* **75,** 298-311 (2019).
4. Hu, Q. *et al.* Predicting equilibrium time by adsorption kinetic equations and modifying Langmuir isotherm by fractal-like approach. *J. Mol. Liq.* **268,** 728-733 (2018).
5. Rudzinski, W. & Plazinski, W. Studies of the kinetics of solute adsorption at solid/solution interfaces: on the possibility of distinguishing between the diffusional and the surface reaction kinetic models by studying the pseudo-first-order kinetics. *J. Phys. Chem. C* **111,** 15100-15110 (2007).
6. Haerifar, M. & Azizian, S. Fractal-like adsorption kinetics at the solid/solution interface. *J. Phys. Chem. C* **116,** 13111-13119 (2012).
7. Sun, Y., Lv, H., Zhou, W. & Zhang, C. Research on hydrogen permeability of polyamide 6 as the liner material for type IV hydrogen storage tank. *Int. J. Hydrog. Energy* **45,** 24980-24990 (2020).

8. Barr, C. D., Giacin, J. R. & Hernandez, R. J. A determination of solubility coefficient values determined by gravimetric and isostatic permeability techniques. *Packag. Technol. Sci.* **13,** 157-167 (2000).

9. Ratnakar, R. & Dindoruk, B. A new technique for simultaneous measurement of nanodarcy-range permeability and adsorption isotherms of tight rocks using magnetic suspension balance. *SPE J.* **24,** 2482-2503 (2019).

10. Gajdoš, J., Galić, K., Kurtanjek, Ž. & Ciković, N. Gas permeability and DSC characteristics of polymers used in food packaging. *Polym. Test.* **20,** 49-57 (2000).

11. Stern, S. A., Gareis, P. J., Sinclair, T. F. & Mohr, P. H. Performance of a versatile variable-volume permeability cell. Comparison of gas permeability measurements by the variable-volume and variable-pressure methods. *J. Appl. Polym. Sci.* **7,** 2035-2051 (1963).

12. Jung, J. K., Kim, I. G., Chung, K. S., Kim, Y. I. & Kim, D. H. Determination of permeation properties of hydrogen gas in sealing rubbers using thermal desorption analysis gas chromatography. *Sci. Rep.* **11,** 17092 (2021).

13. Zheng, Y. *et al.* A review on effect of hydrogen on rubber seals used in the high-pressure hydrogen infrastructure. *Int. J. Hydrog. Energy* **45,** 23721-23738 (2020).

14. Castagnet, S., Nait-Ali, A. & Ono, H. Effect of pressure cycling on decompression failure in *EPDM exposed to high-pressure hydrogen, constitutive models for rubber XI* 4 (CRC Press, 2019).

15. Ono, H., Fujiwara, H. & Nishimura, S. Penetrated hydrogen content and volume inflation in unfilled NBR exposed to high-pressure hydrogen–What are the characteristics of unfilled-NBR dominating them? *Int. J. Hydrog. Energy* **43,** 18392-18402 (2018).

16. Jung, J. K., Kim, I. G. & Kim, K. T. Evaluation of hydrogen permeation characteristics in rubbery polymers. *Curr. Appl. Phys.* **21,** 43-49 (2021).

17. Jung, J. K., Kim, I. G., Kim, K. T., Ryu, K. S. & Chung, K. S. Evaluation techniques of hydrogen permeation in sealing rubber materials. *Polym. Test.* **93,** 107016 (2021).

18. Barth, R. R., Simmons, K. L. & Marchi, C. S. *Polymers for hydrogen infrastructure and vehicle fuel systems: applications, properties, and gap analysis* (Office of Scientific and Technical Information (OSTI), 2013).

19. Crank, J. *The mathematics of diffusion, Brunel University* (Oxford University Press, 1975).

20. Yang, Y. & Liu, S. Estimation and modeling of pressure-dependent gas diffusion coefficient for coal: a fractal theory-based approach. *Fuel* **253,** 588-606 (2019).

21. Nelder, J. A. & Mead, R. A simplex method for function minimization. *Comput. J.* **7,** 308-313 (1965).

22. Fujiwara, H., Yamabe, J. & Nishimura, S. Evaluation of the change in chemical structure of acrylonitrile butadiene rubber after high-pressure hydrogen exposure. *Int. J. Hydrog. Energy* **37,** 8729-8733 (2012).

23. Fujiwara, H. & Nishimura, S. Evaluation of hydrogen dissolved in rubber materials under high-pressure exposure using nuclear magnetic resonance. *Polym. J.* **44,** 832-837 (2012).

24. Li, X. S., Xin, Q., Guo, X. X., Grange, P. & Delmon, B. Reversible hydrogen adsorption on MoS_2 studied by temperature-programmed desorption and temperature-programmed reduction. *J. Catal.* **137,** 385-393 (1992).

25. Mills, G., Jónsson, H. & Schenter, G. K. Reversible work transition state theory: application to dissociative adsorption of hydrogen. *Surf. Sci.* **324,** 305-337 (1995).

26. Enomoto, K. *et al. Radiation cross-linked polyethylene as hydrogen polymer materials* (National Meeting of the Chemical Society of Japan).

27. Nishimura, S. *International symposium of hydrogen polymers team* (Hydrogenius, Shiiki Hall, Kyushu University, 2017).

Acknowledgements

This research was supported by the Development of Reliability Measurement Technology for Hydrogen Refueling Station, which is funded by the Korea Research Institute of Standards and Science (KRISS - 2021 - GP2021-0007).

Author contributions

Jae Kap Jung made a substantial contribution in the design of this work and analysis.

Kyu-Tae Kim made a numerical simulation of measured data.

Un Bong Baek made a contribution in the data analysis and the creation of idea for this work.

Seung Hoon Nahm made a contribution in the determination of direction of the work and project.

Competing interests

The authors declare that they have no known competing financial interests or personal relationships that could have appeared to influence the work reported in this paper.

Figure legends

Fig. 1. (**a**) Schematic diagram of the VAT system in which the cylinder is standing upright and (**b**) photograph of a stretched graduated cylinder with a capacity of 20 ml. The blue part in (**a**) indicates the distilled water filled in the water container and cylinder.

Fig. 2. (**a**) Clockwise sequence for measuring the sorption diffusion parameter. The measurement by VAT is performed after loading inside the graduated cylinder of the rubber exposed to a high-pressure chamber.

Fig. 2. (**b**) Sequence for measuring the desorption diffusion parameter. The measurement by VAT is performed after loading the rubber exposed to a high-pressure chamber inside the graduated cylinder.

Fig. 3. Total hydrogen sorption (C_∞) and desorption content (C_0) versus sample volume for cylindrically shaped (**a**) NBR and (**b**) EPDM exposed to 5.75 MPa and 296 K.

Fig. 4. Comparison of the diffusion coefficients (D_s and D_d) versus sample volume for cylindrically shaped (**a**) NBR and (**b**) EPDM exposed to 5.75 MP and 296 K.

Fig. 5. (**a**) Normalized sorption content versus exposed time and (**b**) desorption content versus time after decompression for cylindrically shaped NBR with a diameter of 5 mm and thickness of 2.5 mm, a diameter of 10 mm and thickness of 2.5 mm, and a diameter of 14 mm and thickness of 2.5 mm. D and T are the diameter and thickness, respectively.

Fig. 6. (**a**) Normalized sorption content versus exposed time and (**b**) normalized desorption content versus time after decompression for a cylindrically shaped NBR with a diameter of 14 mm and thickness of 2.5 mm, a diameter of 12 mm and thickness of 5 mm, and a diameter of 12 mm and thickness of 10 mm. D and T are the diameter and thickness, respectively.

Fig. 7. Three-dimensional plot of (**a**) sorption and (**b**) desorption equilibrium time versus volume for NBR. The number at the top of the bar indicates the aspect ratio (AR) of cylindrical rubber.

Fig. 8. Three-dimensional plot of (**a**) sorption and (**b**) desorption equilibrium time versus volume for EPDM. The number at the top of the bar indicates the aspect ratio (AR) of cylindrical rubber.

Fig. 9. Saturation time for the sorption equilibrium and desorption equilibrium versus the square of the thickness for (**a**) NBR and (**b**) EPDM. The number indicates the aspect ratio (AR) of cylindrical rubber.

Fig. 10. Numerical simulation for (**a**) normalized hydrogen content versus elapsed time with different thicknesses, (**b**) linear correlation between equilibrium time and square of thickness, (**c**) normalized hydrogen content versus elapsed time with different diameters, and (**d**) equilibrium time versus radius with a DC of 5×10^{-11} m^2/s and thickness of 2.5 mm. D and T indicate the diameter and thickness of the specimen, respectively. DC represents diffusion coefficient.

Figures

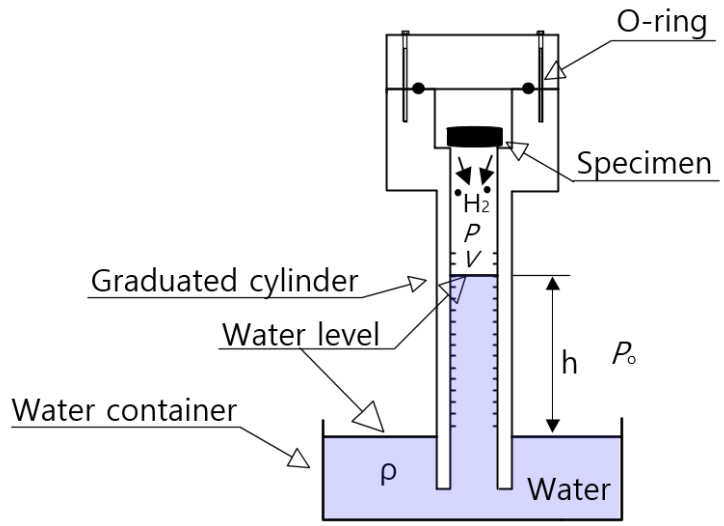

(a)

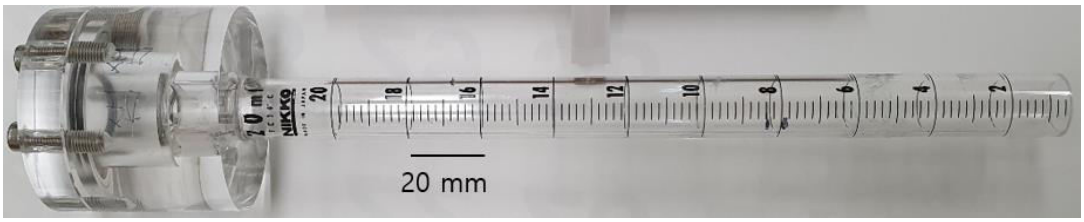

(b)

Fig. 1

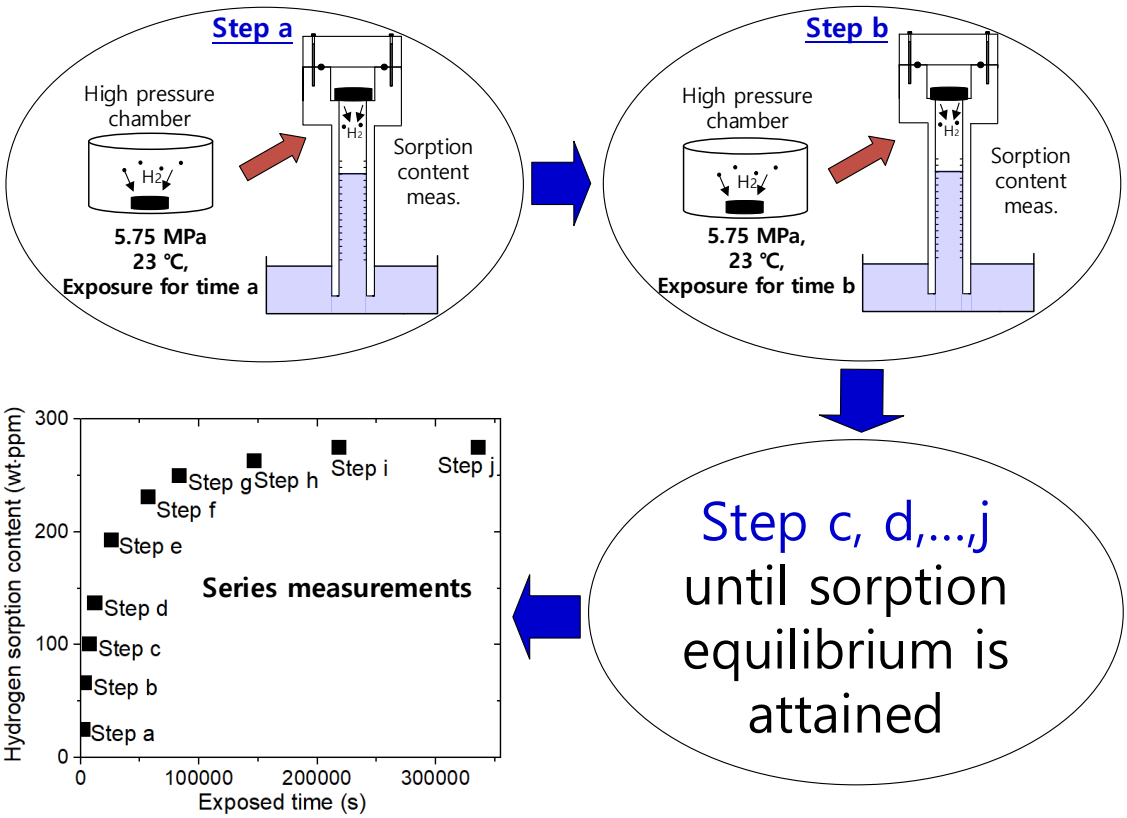
Step a
High pressure chamber
H2
5.75 MPa
23 ℃,
Exposure for time a
Sorption content meas.
Step b
High pressure chamber
H2
5.75 MPa,
23 ℃,
Exposure for time b
Sorption content meas.
Step c, d,…,j
until sorption equilibrium is attained
Hydrogen sorption content (wt-ppm)
Exposed time (s)
Series measurements
Step a
Step b
Step c
Step d
Step e
Step f
Step g
Step h
Step i
Step j
0
100
200
300
0
100000
200000
300000

Fig. 2a

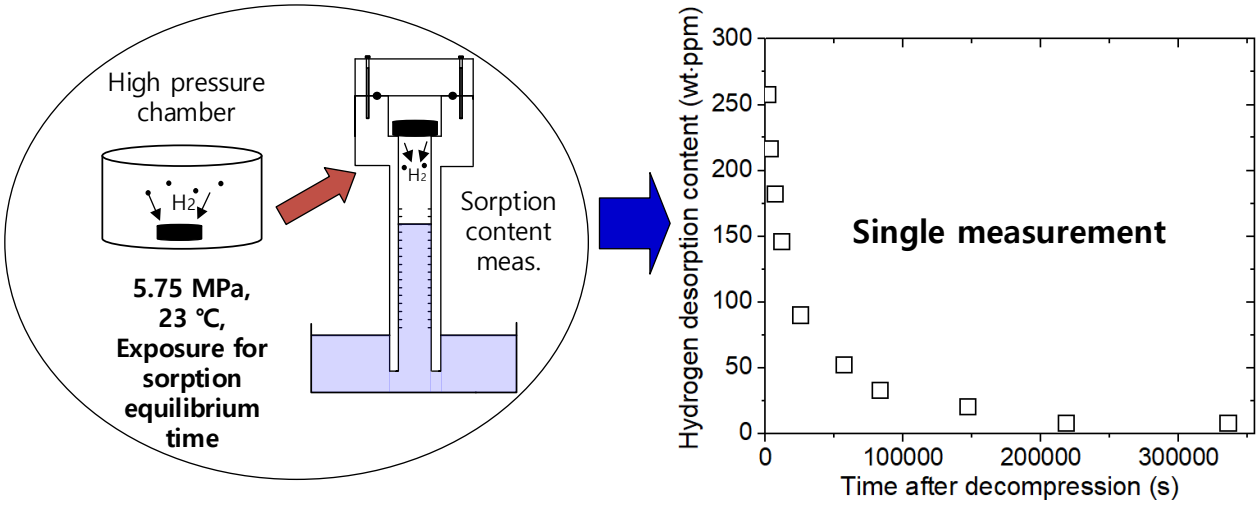
High pressure chamber
H2
5.75 MPa, 23 ℃, Exposure for sorption equilibrium time
H2
Sorption content meas.
Hydrogen desorption content (wt·ppm)
300
250
200
150
100
50
0
Single measurement
0
100000
200000
300000
Time after decompression (s)

Fig. 2b

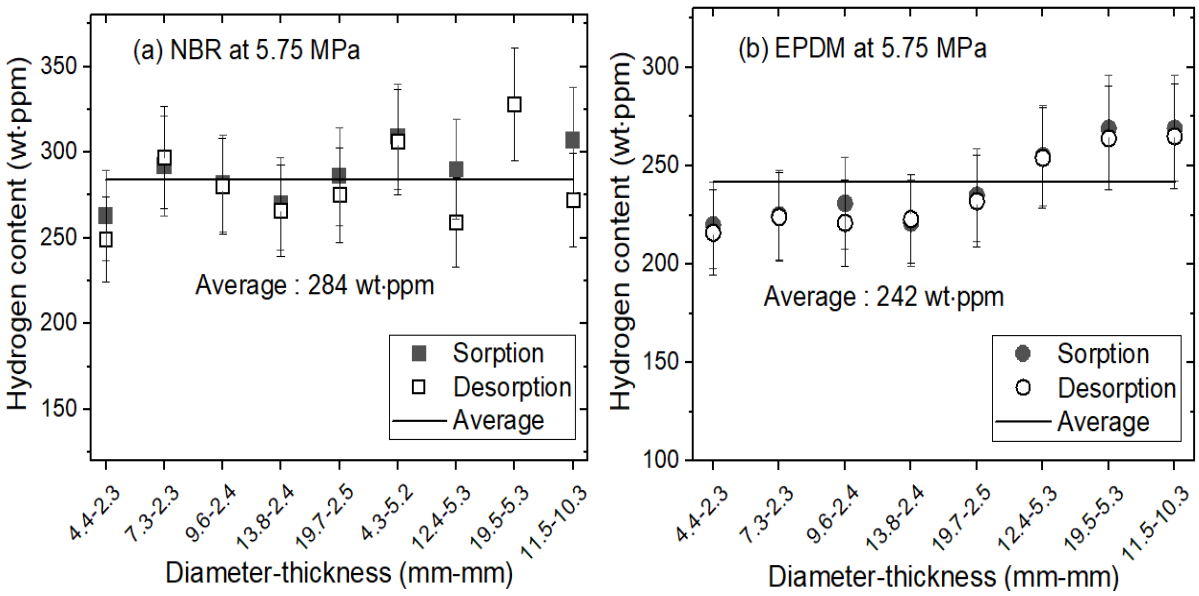
(a) NBR at 5.75 MPa
Hydrogen content (wt·ppm)
350
300
250
200
150
Average : 284 wt·ppm
Sorption
Desorption
Average
4.4-2.3
7.3-2.3
9.6-2.4
13.8-2.4
19.7-2.5
4.3-5.2
12.4-5.3
19.5-5.3
11.5-10.3
Diameter-thickness (mm-mm)
(b) EPDM at 5.75 MPa
Hydrogen content (wt·ppm)
300
250
200
150
100
Average : 242 wt·ppm
Sorption
Desorption
Average
4.4-2.3
7.3-2.3
9.6-2.4
13.8-2.4
19.7-2.5
12.4-5.3
19.5-5.3
11.5-10.3
Diameter-thickness (mm-mm)

Fig. 3

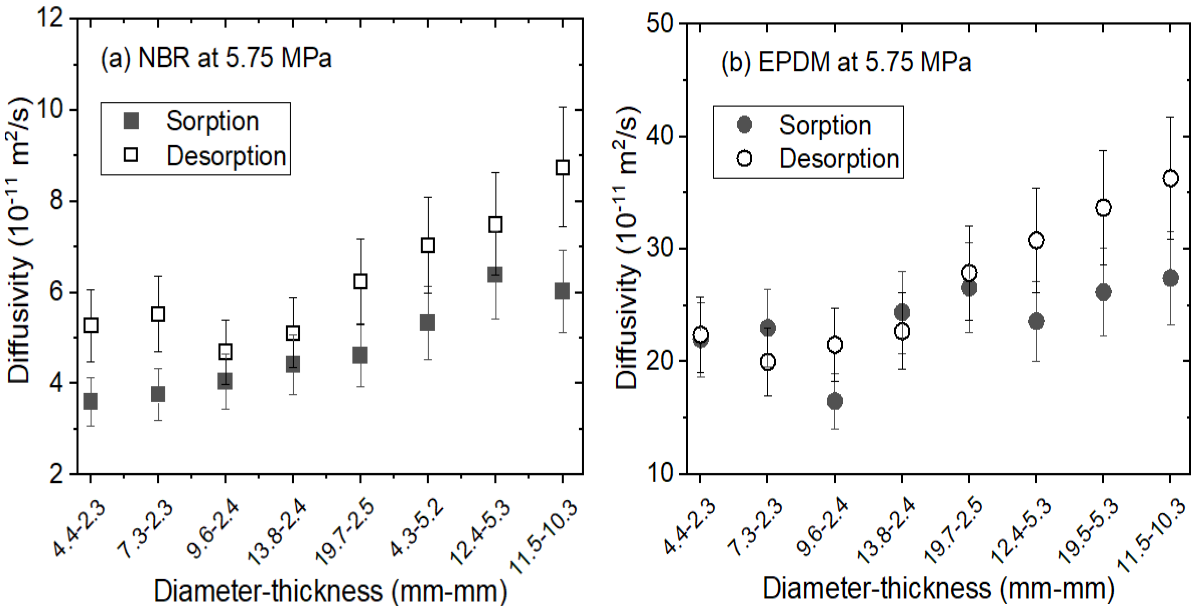
(a) NBR at 5.75 MPa
Sorption
Desorption
Diffusivity (10^{-11} m^2/s)
Diameter-thickness (mm-mm)
4.4-2.3
7.3-2.3
9.6-2.4
13.8-2.4
19.7-2.5
4.3-5.2
12.4-5.3
11.5-10.3
(b) EPDM at 5.75 MPa
Sorption
Desorption
Diffusivity (10^{-11} m^2/s)
Diameter-thickness (mm-mm)
4.4-2.3
7.3-2.3
9.6-2.4
13.8-2.4
19.7-2.5
12.4-5.3
19.5-5.3
11.5-10.3

Fig. 4

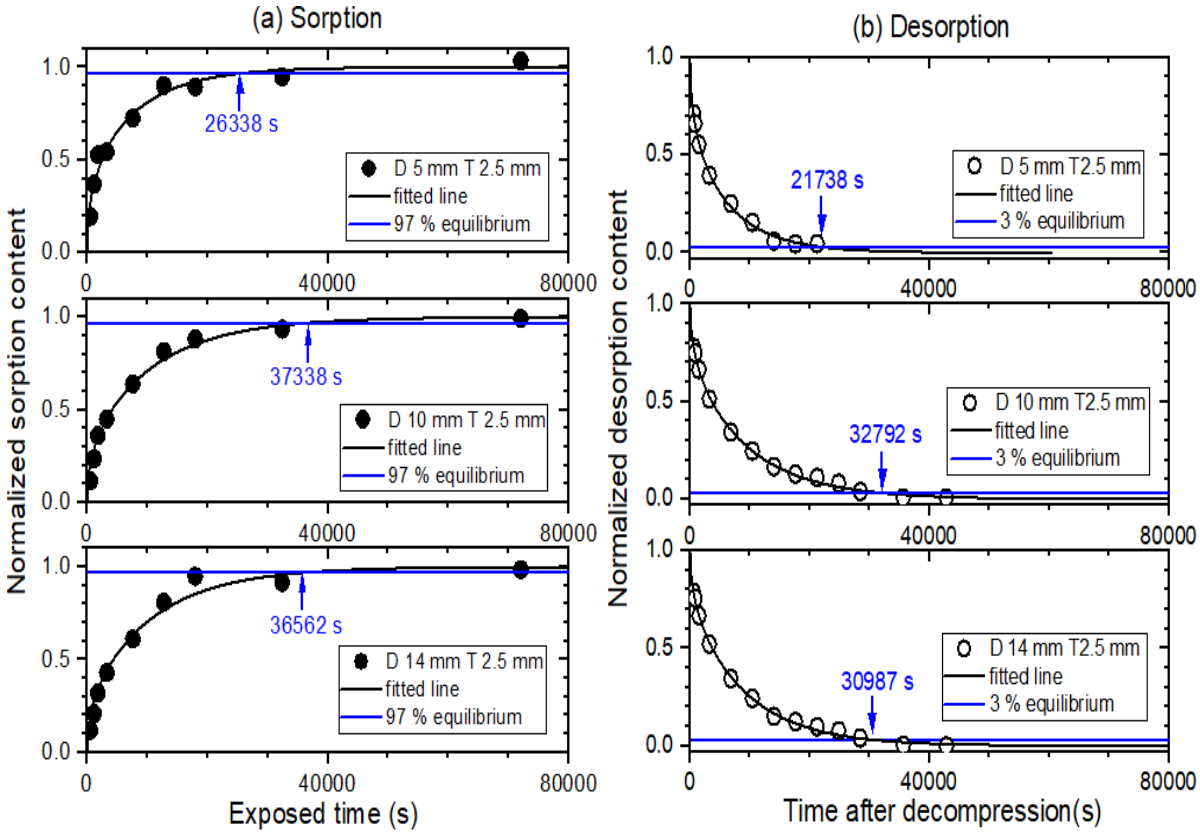
(a) Sorption
(b) Desorption
Normalized sorption content
Normalized desorption content
Exposed time (s)
Time after decompression(s)
26338 s
37338 s
36562 s
21738 s
32792 s
30987 s
D 5 mm T 2.5 mm
D 10 mm T 2.5 mm
D 14 mm T 2.5 mm
D 5 mm T2.5 mm
D 10 mm T2.5 mm
D 14 mm T2.5 mm
fitted line
97 % equilibrium
3 % equilibrium
0.0
0.5
1.0
0
40000
80000

Fig. 5

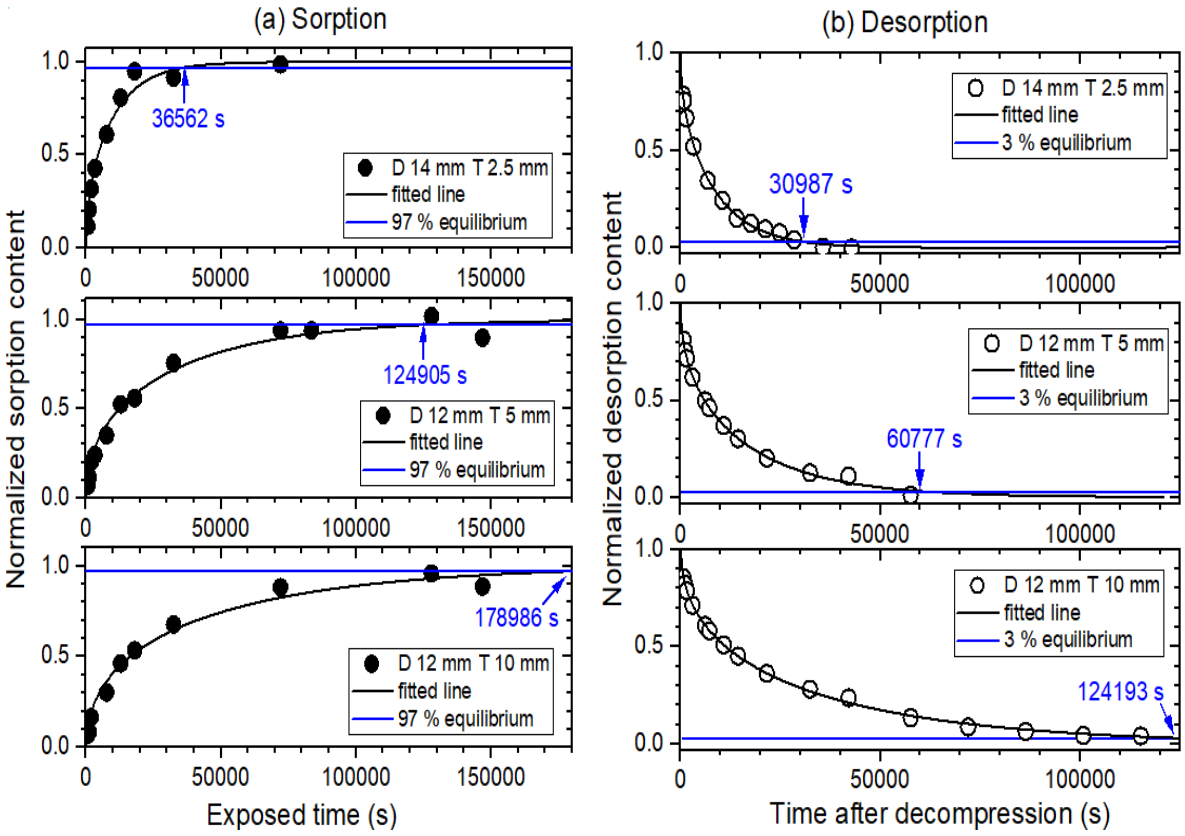
(a) Sorption
(b) Desorption
Normalized sorption content
Normalized desorption content
Exposed time (s)
Time after decompression (s)
D 14 mm T 2.5 mm
fitted line
97 % equilibrium
36562 s
D 12 mm T 5 mm
124905 s
D 12 mm T 10 mm
178986 s
3 % equilibrium
30987 s
60777 s
124193 s

Fig. 6

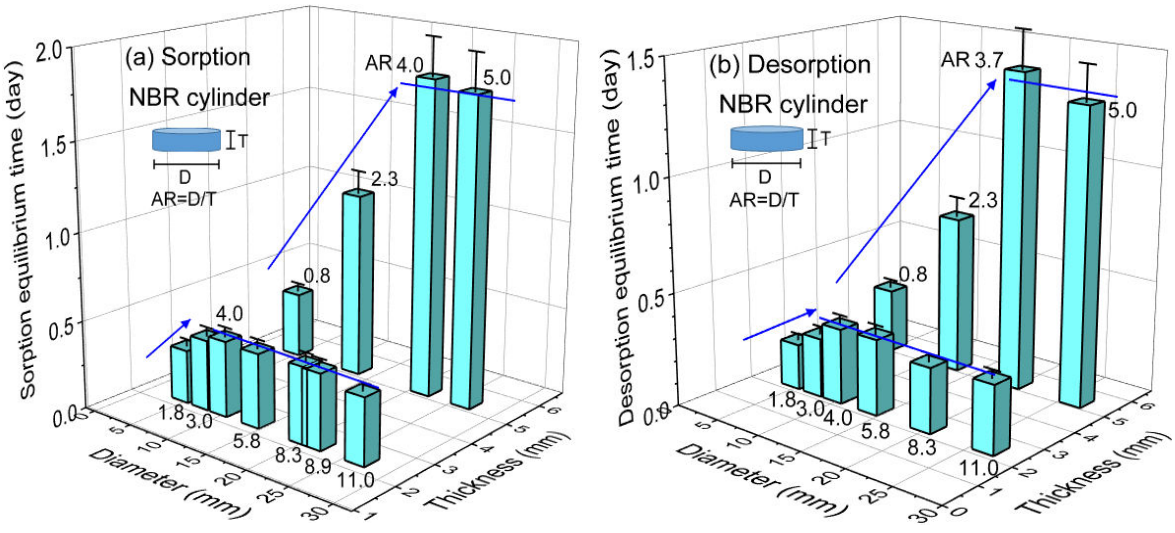
(a) Sorption
NBR cylinder
T
D
AR=D/T
Sorption equilibrium time (day)
Diameter (mm)
Thickness (mm)
AR 4.0
5.0
2.3
0.8
4.0
1.8
3.0
5.8
8.3
8.9
11.0
(b) Desorption
NBR cylinder
T
D
AR=D/T
Desorption equilibrium time (day)
Diameter (mm)
Thickness (mm)
AR 3.7
5.0
2.3
0.8
1.8
3.0
4.0
5.8
8.3
11.0

Fig. 7

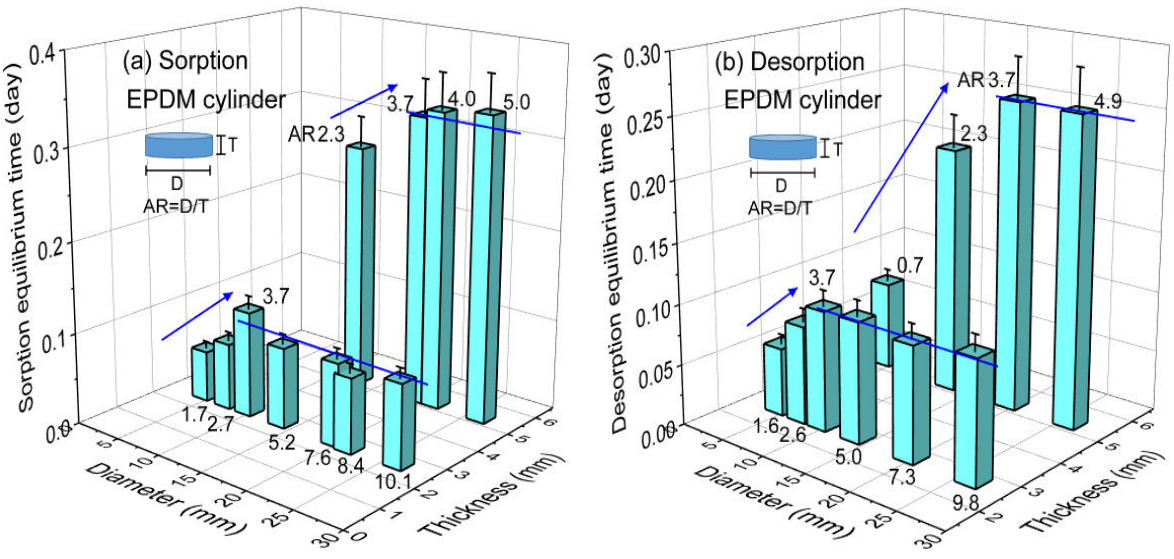
(a) Sorption
EPDM cylinder
T
D
AR=D/T
Sorption equilibrium time (day)
0.4
0.3
0.2
0.1
0.0
AR 2.3
3.7
4.0
5.0
3.7
1.7
2.7
5.2
7.6
8.4
10.1
Diameter (mm)
Thickness (mm)
(b) Desorption
EPDM cylinder
T
D
AR=D/T
Desorption equilibrium time (day)
0.30
0.25
0.20
0.15
0.10
0.05
0.00
AR 3.7
2.3
4.9
3.7
0.7
1.6
2.6
5.0
7.3
9.8
Diameter (mm)
Thickness (mm)

Fig. 8

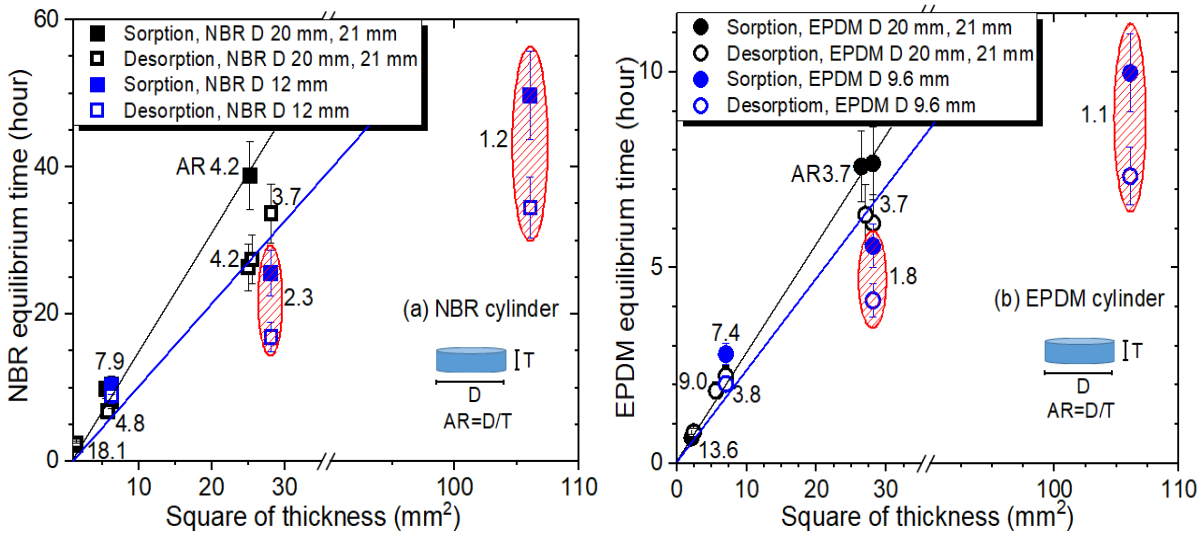
Sorption, NBR D 20 mm, 21 mm
Desorption, NBR D 20 mm, 21 mm
Sorption, NBR D 12 mm
Desorption, NBR D 12 mm
NBR equilibrium time (hour)
Square of thickness (mm2)
AR 4.2
3.7
4.2
2.3
1.2
7.9
4.8
18.1
(a) NBR cylinder
T
D
AR=D/T
Sorption, EPDM D 20 mm, 21 mm
Desorption, EPDM D 20 mm, 21 mm
Sorption, EPDM D 9.6 mm
Desorptiom, EPDM D 9.6 mm
EPDM equilibrium time (hour)
Square of thickness (mm2)
AR3.7
3.7
1.8
1.1
7.4
9.0
3.8
13.6
(b) EPDM cylinder
T
D
AR=D/T

Fig. 9

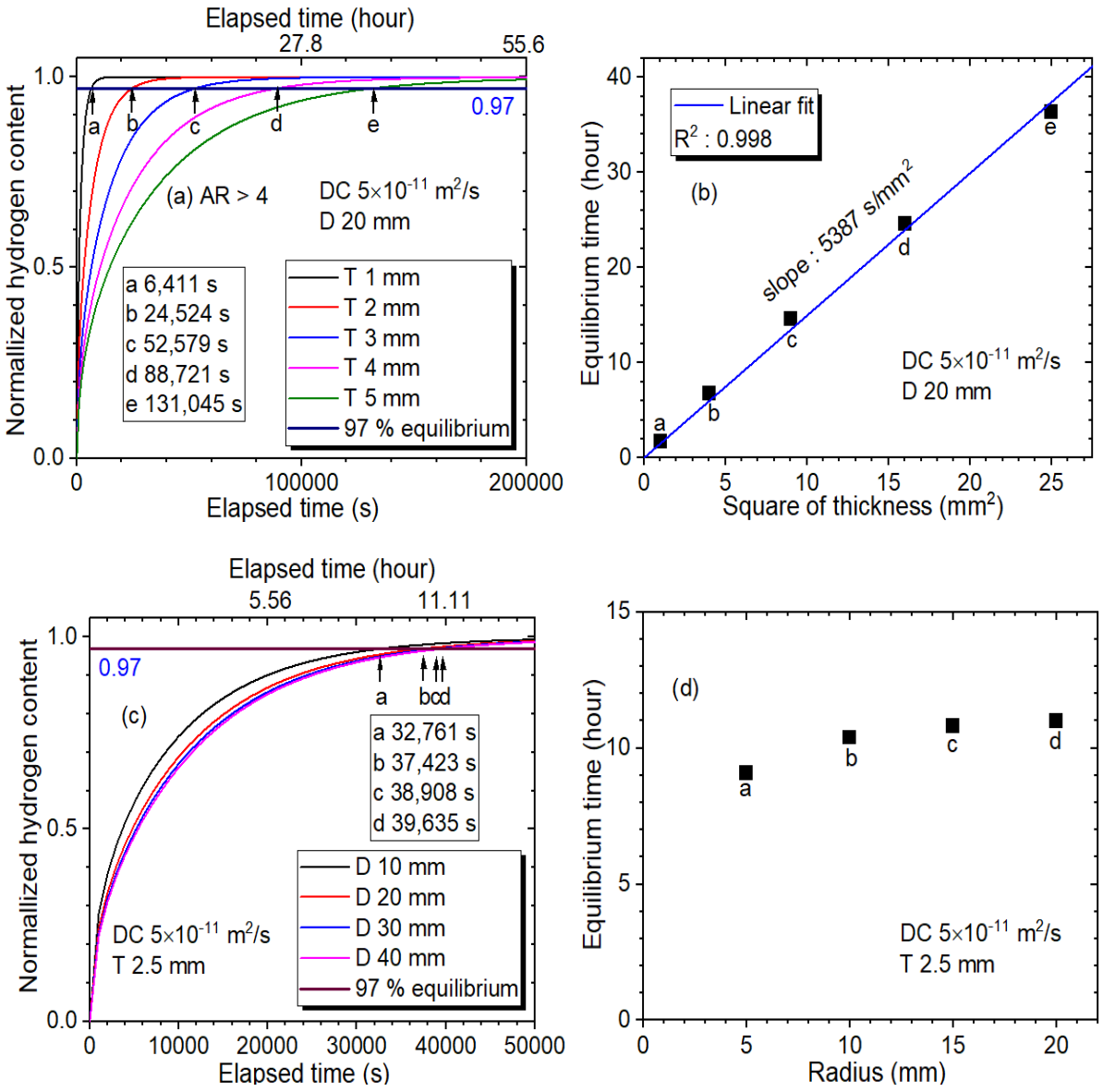
Elapsed time (hour)
27.8
55.6
Normallized hydrogen content
1.0
0.5
0.0
0.97
a
b
c
d
e
(a) AR > 4
DC 5×10-11 m2/s
D 20 mm
a 6,411 s
b 24,524 s
c 52,579 s
d 88,721 s
e 131,045 s
T 1 mm
T 2 mm
T 3 mm
T 4 mm
T 5 mm
97 % equilibrium
0
100000
200000
Elapsed time (s)
Equilibrium time (hour)
40
30
20
10
0
Linear fit
R2 : 0.998
(b)
slope : 5387 s/mm2
DC 5×10-11 m2/s
D 20 mm
0
5
10
15
20
25
Square of thickness (mm2)
Elapsed time (hour)
5.56
11.11
0.97
(c)
a
bcd
a 32,761 s
b 37,423 s
c 38,908 s
d 39,635 s
DC 5×10-11 m2/s
T 2.5 mm
D 10 mm
D 20 mm
D 30 mm
D 40 mm
97 % equilibrium
0
10000
20000
30000
40000
50000
Elapsed time (s)
15
10
5
0
(d)
DC 5×10-11 m2/s
T 2.5 mm
0
5
10
15
20
Radius (mm)

Fig. 10